



# Intratumoral CXCL13<sup>+</sup> CD160<sup>+</sup> CD8<sup>+</sup> T cells promote the formation of tertiary lymphoid structures to enhance the efficacy of immunotherapy in advanced gastric cancer

Jiawei Wang,<sup>1</sup> Yuan Liang ,<sup>2</sup> Ao Xue,<sup>1</sup> Jian Xiao,<sup>1</sup> Xinyu Zhao,<sup>1</sup> Shuqing Cao,<sup>1</sup> Pengyu Li,<sup>1</sup> Jiacheng Dong,<sup>1</sup> Yuan Li,<sup>1</sup> Zekuan Xu,<sup>1</sup> Li Yang <sup>1</sup>

**To cite:** Wang J, Liang Y, Xue A, *et al.* Intratumoral CXCL13<sup>+</sup> CD160<sup>+</sup> CD8<sup>+</sup> T cells promote the formation of tertiary lymphoid structures to enhance the efficacy of immunotherapy in advanced gastric cancer. *Journal for ImmunoTherapy of Cancer* 2024;**12**:e009603. doi:10.1136/jitc-2024-009603

► Additional supplemental material is published online only. To view, please visit the journal online (<https://doi.org/10.1136/jitc-2024-009603>).

JW, YLiang, AX and JX contributed equally.

Accepted 19 August 2024



© Author(s) (or their employer(s)) 2024. Re-use permitted under CC BY-NC. No commercial re-use. See rights and permissions. Published by BMJ.

<sup>1</sup>Department of General Surgery, The First Affiliated Hospital of Nanjing Medical University, Nanjing, Jiangsu, China

<sup>2</sup>Southeast University, Nanjing, Jiangsu, China

## Correspondence to

Dr Li Yang;  
pwkyangli@njmu.edu.cn

## ABSTRACT

**Background** Stage IV gastric cancer is a highly heterogeneous and lethal tumor with few therapeutic strategies. The combination of programmed cell death protein 1 inhibitors and chemotherapy is currently the standard frontline treatment regimen for advanced gastric cancer. Nevertheless, it remains a great challenge to screen the beneficiaries of immunochemotherapy and expand indications for this treatment regimen.

**Methods** We conducted a pathological assessment to ascertain the importance of tertiary lymphoid structures based on the tissue samples collected from patients with stage IV gastric cancer (n=15) both prior to and following immunochemotherapy treatment. Additionally, we used spatial (n=10) and single-cell transcriptional analysis (n=97) to investigate the key regulators of tertiary lymphoid structures (TLSs). Multiplex immunofluorescence and image analysis (n=34) were performed to explore the association between tumor-infiltrating CXCL13<sup>+</sup> CD160<sup>+</sup> CD8<sup>+</sup> T cells and TLSs. The relationship between CXCL13<sup>+</sup> CD160<sup>+</sup> CD8<sup>+</sup> T cells and the responsiveness to immunotherapy was also evaluated by multiplex immunofluorescence and image analysis approaches (n=15). Furthermore, we explored the intrinsic characteristics of CXCL13<sup>+</sup> CD160<sup>+</sup> CD8<sup>+</sup> T cells through various experimental techniques, including quantitative reverse transcription-PCR, western blot, and flow cytometry.

**Results** We found that responders exhibited higher levels of TLSs and CXCL13<sup>+</sup> CD160<sup>+</sup> CD8<sup>+</sup> T cells in biopsy tissues prior to immunochemotherapy compared with non-responders. Following conversion therapy, responders also had a higher percentage of mature TLSs and a higher number of CXCL13<sup>+</sup> CD160<sup>+</sup> CD8<sup>+</sup> T cells in surgical resections. Moreover, we discovered that vitamin B<sub>6</sub> in CD160<sup>+</sup> CD8<sup>+</sup> T cells could reduce the ubiquitination modification of HIF-1 $\alpha$  by MDM2, thereby attenuating the degradation of HIF-1 $\alpha$ . Consequently, this led to the transcriptional upregulation of CXCL13 expression, facilitating the recruitment of CXCR5<sup>+</sup> B cells and the formation of TLSs.

**Conclusion** The number and maturity of TLSs, along with the extent of CXCL13<sup>+</sup> CD160<sup>+</sup> CD8<sup>+</sup> T-cell infiltration, might function as potential indicators for assessing the effectiveness of immunotherapy in treating gastric

## WHAT IS ALREADY KNOWN ON THIS TOPIC

⇒ Tertiary lymphoid structures (TLSs) have been reported to be associated with extended survival in gastric cancer. However, there is a paucity of research investigating the underlying mechanisms governing TLSs in gastric malignancies. Meanwhile, there is still insufficient robust evidence to establish the correlation between TLSs and immunotherapy responsiveness in advanced gastric cancer.

## WHAT THIS STUDY ADDS

⇒ Our study was the first to propose that the number and maturity of TLSs, along with the extent of CXCL13<sup>+</sup> CD160<sup>+</sup> CD8<sup>+</sup> T-cell infiltration, could serve as novel biomarkers for immunotherapy in gastric cancer. We also identified that vitamin B<sub>6</sub> supplementation could substantially enhance the efficacies of cancer immunotherapies. Moreover, we demonstrated vitamin B<sub>6</sub> could promote the secretion of CXCL13 by CD160<sup>+</sup> CD8<sup>+</sup> T cells by reducing the degradation of HIF-1 $\alpha$ , thereby promoting the formation of TLSs.

## HOW THIS STUDY MIGHT AFFECT RESEARCH, PRACTICE OR POLICY

⇒ Our study was expected to refine the theory of immunotherapy and shed important new light on the clinical application of a more effective immunotherapy for advanced gastric cancer.

malignancies. Furthermore, our research suggests that vitamin B<sub>6</sub> could enhance the secretion of CXCL13 by CD160<sup>+</sup> CD8<sup>+</sup> T cells by reducing the degradation of HIF-1 $\alpha$ . Additionally, we demonstrate that vitamin B<sub>6</sub> supplementation or targeting pyridoxal kinase could substantially improve the efficacy of immunotherapies for gastric cancer.

## INTRODUCTION

Gastric cancer is among the most prevalent malignancies worldwide, occupying the fifth position in terms of tumor incidence and the

fourth in mortality worldwide.<sup>1</sup> Over 70% of individuals with gastric cancer are diagnosed at locally advanced or metastatic stages in China. The overall prognosis of patients with gastric cancer is poor due to a high proportion of patients with advanced disease. Furthermore, effective treatment options for these patients remain lacking. Systemic chemotherapy as initial therapy is the mainstay of treatment for advanced gastric cancer. However, the median survival time is still limited to approximately 15 months when patients are treated with chemotherapy alone.<sup>2</sup>

Recently, several cohort studies have validated the effectiveness of programmed cell death protein 1 (PD-1) inhibitors plus chemotherapy in the first-line treatment of advanced gastric cancer.<sup>3–7</sup> Additionally, conversion surgery has demonstrated the potential to prolong survival by over 20 months in patients with stage IV gastric cancer who have achieved a satisfactory clinical response to immunochemotherapy.<sup>8</sup> Nonetheless, there is still a considerable unmet need for higher efficacy rates. Due to intratumor heterogeneity, only a few patients derived benefits from this treatment regimen. Therefore, it is absolutely imperative to screen the predominant beneficiary population and reverse the refractoriness in patients treated with immunochemotherapy.

Yoshida *et al* had categorized patients with stage IV gastric cancer into four groups based on anatomical relationships and surgical techniques. Although this classification aids in selecting appropriate candidates for conversion therapy, its precision is limited according to the follow-up results.<sup>9</sup> Thus, precise molecular stratification of stage IV gastric cancer is necessary. The efficacy of immunochemotherapy is strongly linked to the response to immune checkpoint inhibitors, especially PD-1 inhibitors. A series of biomarkers represented by microsatellite instability-high (MSI-H) / mismatch repair deficiency (dMMR) status and programmed cell death-ligand 1 (PD-L1) expression have been frequently used to predict the response to PD-1 inhibitors in gastric cancer. Nevertheless, the incidence of MSI-H/dMMR gastric cancer is low and reported to be 5–15%.<sup>10</sup> Additionally, PD-L1 expression is not an optimal biomarker for anti-PD-1 therapies. Even if the combined positive score exceeds 10, approximately 30% of patients with microsatellite stability (MSS) gastric cancer would not benefit from immunochemotherapy.<sup>11</sup> Thus, it is crucial to discover novel biomarkers for immunotherapy. Additionally, identifying new molecular targets to reverse the refractoriness is also an urgent priority for non-responders.

Tertiary lymphoid structures (TLSs) are lymphoid-like structures formed in chronically inflamed non-lymphoid tissues, including tumors.<sup>12</sup> Effector T cells and high-affinity antibodies within TLSs could directly target and eliminate tumor cells because TLSs are not encased in membranes. Previous studies have demonstrated that a high density of TLSs was associated with extended survival in gastric cancer.<sup>13 14</sup> Apart from that, it has been reported that TLSs and B cells were implicated in the

response to immunotherapy across various tumors, such as melanoma,<sup>15</sup> renal cell carcinoma,<sup>16</sup> head and neck squamous cell carcinoma<sup>17</sup> and sarcoma.<sup>18</sup> However, the relationship between TLSs and immunotherapy efficacy in gastric cancer remains largely unexplored. Moreover, inducing the formation or maturation of TLSs represents an effective anticancer strategy with promising clinical implications.<sup>19</sup> Nonetheless, there are currently no safe and effective agents available for inducing TLS formation in cancer treatment. Of note, CXCL13 has been reported to be essential for TLS formation. Moreover, CXCL13 played a critical role in the humoral immune response and the maintenance of the germinal center.<sup>20</sup> With the development of single-cell sequencing, new T-cell subpopulations, such as CXCL13<sup>+</sup> T cells, were continually identified. Multiple studies have shown that intratumoral CXCL13<sup>+</sup> T cells could recruit B lymphocytes to promote TLS formation and maturation.<sup>21 22</sup> However, the characteristics and the cell-intrinsic regulatory mechanisms of these CXCL13<sup>+</sup> T cells remain elusive. Moreover, investigating the mechanisms of CXCL13<sup>+</sup> T cell-B-cell interactions could provide novel ideas about TLS-inducing agents.

In this research, we assessed tumor infiltration by diverse immune cell phenotypes, including TLSs and CXCL13<sup>+</sup> T-cell populations, in tissue samples obtained before and after immunochemotherapy from patients with advanced gastric cancer. Additionally, we found that vitamin B<sub>6</sub> supplementation or targeting pyridoxal kinase (PDXK) could boost the efficacy of immunotherapy primarily promoting the formation of TLSs through the upregulation of CXCL13 expression in CXCL13<sup>+</sup> CD160<sup>+</sup> CD8<sup>+</sup> T cells. This study will provide new insights into the treatment of advanced gastric cancer.

## METHODS

### Data collection

The gastric cancer single-cell RNA sequencing (scRNA-seq) data sets used in this research were obtained from GSE206785, GSE167297, GSE150290, and GSE183904 which were from GEO database (<https://www.ncbi.nlm.nih.gov/geo/>), CRA002586 which was from the Genome Sequence Archive (<https://ngdc.cncb.ac.cn/gsa/browse/CRA002586>), and another scRNA data set was submitted by Anuja Sathe *et al*. We collected and collated the expression profile, along with the clinical information of the ARCG cohort (GSE66229), which contained 300 gastric cancer samples. We gathered the spatial transcriptome sequencing data from nine primary gastric cancer samples and one peritoneal metastatic lesion from GSE251950.

### Spatial transcriptomics analysis

The gene-spot matrices generated after spatial transcriptomic (ST) data processing from ST and visium samples were analyzed with the Seurat package (V.4.1.1) in R. Spots were filtered for a minimum detected gene count of 200

genes. In contrast, genes with fewer than 10 read counts or expressed in fewer than 3 spots were removed. Normalization across spots was performed with the LogVMR function. Dimensionality reduction and clustering were performed with independent principal component analysis (PCA) with the first 30 principal components (PCs). We collected TLS-50 signatures from Wu *et al* in online supplemental table S1<sup>23</sup> and then applied the “AddModuleScore” function with default parameters in the Seurat package to calculate the gene scores of the TLSs. The cell type signature score derived from the scRNA-seq data set was added to “metadata” of the ST data set with the “AddModulScore” function with default parameters in Seurat. Spatial feature expression plots were generated with the “SpatialFeaturePlot” function in the Seurat package. We applied the SpaGene method to identify distinct clusters for each sample.

### Single-cell transcriptome analysis

Cell Ranger (V.6.0.2) was used to read mapping and gene expression quantification. Seurat package (V.4.1.1) was applied for downstream analysis. Cells with less than 1,000 unique molecular identifiers (UMIs) or >15% mitochondria genes were excluded. Doublets were assessed using the DoubletFinder (V.2.0.3) algorithm for each sample. We used single-cell variational inference (scVI) tools to remove batch effects to ensure that our single-cell analysis was not unduly driven by the outlying characteristics of one or a few patients’ transcriptional profiles. We scaled data with the top 4,000 most variable genes by using the FindVariableFeatures function and used variable genes for PCA, used FindNeighbors to get nearest neighbors for graph clustering based on the top 50 PCs, and used FindCluster to obtain cell subtypes, and visualized cells with the Uniform Manifold Approximation and Projection (UMAP) algorithm. Then, we filtered T cells based on CD3D, CD3E, and CD3G expression and used FindCluster to obtain T-cell subtypes.

### Clinical samples and TLSs assessment

In this study, 116 clinical advanced gastric cancer tissues were obtained from patients who underwent radical gastrectomy at the First Affiliated Hospital of Nanjing Medical University between 2016 and 2018 and none of these patients were treated with neoadjuvant chemotherapy or immunotherapy. Additionally, 15 gastric cancer tissues from patients who received immunotherapy combined with chemotherapy were obtained between 2019 and 2024, either from radical gastrectomy or preoperative gastroscopy with gastric biopsy at the same institution. The immunotherapy regimens included camrelizumab, nivolumab, tislelizumab, sintilimab. The chemotherapy regimens included oxaliplatin plus calcium levofolinate, 5-fluorouracil, S-1 plus oxaliplatin, oxaliplatin plus capecitabine, 5-fluorouracil plus leucovorin, oxaliplatin, and docetaxel. Trastuzumab was recommended for patients with HER2-positive cancers. The tumor regression grade (TRG) was evaluated by

experienced pathologists according to the American Joint Committee on Cancer/College of American Pathologists system. TRG 0 means a complete response (CR), with no residual tumor cells and fibrosis extending through the different layers of the gastric wall. The details for these 15 patients are shown in table 1.

The pathological assessment of TLSs was primarily based on H&E-stained slides. TLSs are defined as dense lymphocyte aggregates (>100 cells) located among tumor cells or tumor fibrosis area. Furthermore, TLSs are characterized as a dense aggregation of unencapsulated B cells (CD20), accompanied by an adjacent T-cell zone (CD4 and CD8). Therefore, we performed immunohistochemistry (IHC) staining in some cases to adequately reveal the morphology and spatial distribution of the constituent cells of TLSs. These samples were incubated with anti-CD20, anti-CD8 or anti-CD4. The TLS histological scoring system was applied to gastric cancer tissues based on the results of IHC and H&E staining. The scoring system includes two aspects: (1) the number of TLS (N); (2) the ratio of TLS area versus tumor area (TLS %). The formula for TLS score was as follows: Score=N×TLS %.

### Multiplex immunofluorescence

The prepared formalin-fixed and paraffin-embedded (FFPE) sections (4µm) were first incubated in a dry oven and then immersed in xylene for deparaffinization. Rehydration was also performed. The sections were then placed with Tris-EDTA buffer for antigen retrieval. After cooled to room temperature (RT), slides were immersed in peroxidase-blocking solution to block endogenous peroxidase activity. Subsequently, multiplex immunofluorescence (mIF) kit (BioMed World, WAS15021) was used for staining. The slides were incubated with the primary antibodies at 4°C overnight. Then, slides were incubated with horseradish peroxidase (HRP)-conjugated secondary antibodies at room temperature. A quick wash in 1× phosphate buffered solution (PBS) buffer was followed by incubation with an appropriate fluorophore-conjugated tyramide signal amplification (TSA) at RT. Again, the slides were exposed to microwave treatment to strip the tissue-bound primary/secondary antibody complexes and ready for labeling of the next marker. The primary antibodies (CD8, Abcam, 1:1000; CD20, Proteintech, 1:2000; CXCL13, Abcam, 1:2000; CD160, Abcam, 1:500; CD4, CST, 1:2000; PDCD1, Proteintech, 1:5000; CXCR5, Abcam, 1:1000), HRP-conjugated secondary antibodies (BioMed World, WAS12011), and fluorophore-conjugated TSA (TSA570, WAS10031; TSA520, WAS10021; TSA620, WAS10041; TSA690, WAS10061) were repeated until all markers were labeled. Finally, the slides were added with 4', 6-diamidino-2-phenylindole (DAPI) in the dark at RT and mounted with anti-fade mounting medium. The PANNORAMIC MIDI II (3DHISTECH) was used to take images of tissue samples.

**Table 1** Basic information about 15 patients with stage IV gastric cancer who received immunochemotherapy as the initial treatment option

No.	Gender	Age	Regimens	Clinical stage (first)	Sites of distant metastases	postoperative pathological examination
1	Male	≥60	SOX+camrelizumab	T4N3M1	Liver metastasis	PR
2	Male	<60	FLOT+nivolumab	T4N2M1	Peritoneal metastasis	SD
3	Male	≥60	CapeOX+trastuzumab+tislelizumab	T3N2M1	Liver metastasis	PR
4	Female	<60	SOX+sintilimab	T4N3M1	Pancreatic metastasis and transverse mesocolon metastasis	SD
5	Female	≥60	CapeOX+tislelizumab	T4N3M1	Peritoneal metastasis	PR
6	Male	≥60	SOX+camrelizumab	T4N2M1	Liver metastasis	CR
7	Female	≥60	FOLFOX+sintilimab	T4N3M1	Liver metastasis	CR
8	Female	≥60	CapeOX+tislelizumab	T4N3M1	Pancreatic metastasis and para-aortic lymph node metastasis	PR
9	Male	<60	CapeOX+trastuzumab+Sintilimab	T4N2M1	Liver metastasis	SD
10	Male	<60	SOX+nivolumab	T4N3M1	Liver metastasis	CR
11	Female	<60	FLOT+tislelizumab	T4N2M1	Peritoneal metastasis	PR
12	Male	≥60	SOX+nivolumab	T4N3M1	Peritoneal metastasis	PR
13	Female	<60	SOX+nivolumab	T4N3M1	Peritoneal metastasis	SD
14	Male	≥60	CapeOX+sintilimab	T4N3M1	Liver metastasis and peritoneal metastasis	-*
15	Female	<60	SOX+nivolumab	T4N3M1	Peritoneal metastasis	-

\*Clinical assessment revealed disease progression and these two patients did not undergo surgery (post-treatment samples were not available).

CapeOX, oxaliplatin plus capecitabine ; CR, complete response; FLOT, 5-fluorouracil plus leucovorin, oxaliplatin, and docetaxel; FOLFOX, 5-fluorouracil; PR, partial response; SD, stable disease; SOX, S-1 plus oxaliplatin.

### Metabolic activity analysis

The R package scMetabolism (V.0.2.1) assesses sets of genes from metabolic pathways to quantify the metabolic activity of single cells based on the scRNA-seq expression matrix. The scMetabolism analysis was performed with Kyoto Encyclopedia of Genes and Genomes (KEGG) metabolism pathways and the VISION quantifying method.

### Mice

Female and male mice (6–8 weeks) were used for all experiments. The 615 and C57BL/6 mouse strains were procured from the Shanghai Laboratory Animal Research Center. On acquisition, a 1-week acclimatization period was provided in a pathogen-free housing environment. For subcutaneous xenograft experiments, either  $1 \times 10^6/100 \mu\text{L}$  mouse forestomach carcinoma (MFC) cells (MeisenCTCC, CTCC-400–0334) or MFC-Luciferase cells (MeisenCTCC, CTCC-0497-Luc2) were digested and resuspended in PBS before being subcutaneously injected into 615 mice (with six mice per treatment group). The calculation of tumor volume was performed using the following formula: volume ( $\text{mm}^3$ ) = width<sup>2</sup> × length/2. In

orthotopic xenograft experiments, tissue blocks ( $1 \text{ mm}^3$ ) obtained from subcutaneous tumors were surgically transplanted into the stomach wall of 615 mice (with six mice per treatment group). The spontaneous gastric cancer model was created by exposing C57BL/6 mice to 240 ppm N-methyl-N-nitrosourea (MNU) in their drinking water.

The diet (from Jiangsu Xietong Pharmaceutical Bio-engineering) was strictly defined as non-VB6 diet, normal-VB6 diet, and excessive-VB6 diet, which contain 0, 6 mg, and 60 mg of vitamin B<sub>6</sub> per kg diets, respectively. Mice were treated with anti-PD-1 antibody intraperitoneally (200  $\mu\text{g}/\text{mouse}$ , every 3 days, Bio X Cell) or MS023 (2 mg/mouse, every day, Selleck) 1 week after subcutaneous injection of tumor cells or orthotopic transplantation. PBS was used as a negative control.

### Patient-derived tumor fragments

Gastric cancer samples were collected from patients undergoing gastrectomy. The samples were diced into approximately 1 mm diameter fragments and then incorporated into an artificial extracellular matrix within a 96-well plate (Corning). The composition of the artificial extracellular

matrix was elaborated below: 10% fetal bovine serum (FBS) - Dulbecco's Modified Eagle's Medium (DMEM) containing 1× Eagle's minimal essential medium (MEM) non-essential amino acids (Sigma-Aldrich), 1 mg/mL collagen I (Corning) and 4 mg/mL phenol red-free ice-cold Matrigel (BD Biosciences). Patient-derived tumor fragments (PDTFs) cultures were stimulated with 10 µg/mL anti-PD-1 alone (Selleck, Sintilimab), 0.5 mM pyridoxal alone (Selleck), or the combination of anti-PD-1 and pyridoxal where indicated.

### Analysis of secreted mediators

The supernatants of PDTFs cultures were collected after 48 hours of culture. The indicated cytokines and chemokines within the supernatants were detected using human IL-2 ELISA Kit (Solarbio, SEKH-0008), human IFN-γ ELISA Kit (Solarbio, SEKH-0046), human CXCL13 ELISA Kit (Solarbio, SEKH-0072) and human TNF-α ELISA Kit (Solarbio, SEKH-0047) according to the manufacturers' instructions.

### Statistical analysis

The data analysis was performed using GraphPad Prism V.10.0.2 software and SPSS V.27.0.1. Statistical significance was assessed employing two-tailed unpaired t-tests for comparing two groups, while one-way analysis of variance followed by Bonferroni's multiple comparisons test was used for comparisons involving more than two groups. The results of in vitro functional assays were reported based on a minimum of three independent experiments and were expressed as mean±SD.

Additional experimental procedures are provided in the online supplemental information.

## RESULTS

### The abundance and maturation of intratumoral TLSs were associated with improved prognosis and the efficacy of immunochemotherapy

Previous studies have demonstrated that a high enrichment of TLSs may prolong the survival of patients with gastric cancer.<sup>13,14</sup> Initially, we evaluated the abundance of TLSs in tumor tissues from 116 patients with gastric cancer (table 2) and observed that the TLSs-high group had a superior outcome compared with the TLSs-low group (online supplemental figure S1A). Therefore, TLSs could serve as a prognostic biomarker for gastric cancer. Then, we began to investigate whether TLSs could be used as biomarkers to predict the efficacy of immunotherapy in advanced gastric cancer. Accordingly, we conducted a retrospective analysis using gastroscopic biopsies obtained from patients with stage IV gastric cancer prior to initiating immunotherapy (table 1). The results revealed a positive correlation between the response to immunotherapy and the density of intratumoral TLSs before treatment initiation (online supplemental figure S1B). Therefore, TLSs could be used as an

index in the evaluation of immunotherapeutic effect in advanced gastric cancer.

Subsequently, we set out to interrogate the effect of immunochemotherapy on the formation and maturation of TLSs. We found that the number of intratumoral TLSs increased after treatment (online supplemental figure S1C). Then, we classified the TLSs into three maturity levels based on expression of the markers CD23<sup>+</sup>: (1) lymphoid aggregates with no evidence of CD23<sup>+</sup> mature follicular dendritic cells (mFDC); (2) primary follicles containing scattered CD23<sup>+</sup> mFDC; and (3) mature TLSs, which are secondary follicles with a meshwork of CD23<sup>+</sup> mFDC (online supplemental figure S1D). We found that patients with a partial response (PR) had a higher proportion of intratumoral mature TLSs after treatment compared with patients with a poor response (online supplemental figure S1E). However, these phenomena were not obvious in patients with a CR. We speculated that this might be attributed to the absence of sustained antigen stimulation for a long period before detection.

To further validate the impact of TLSs on gastric cancer development, we calculated the gene scores of TLSs in the spatial transcriptome data of gastric cancer and observed the presence of apparent TLS regions. Consistent with previous reports, TLSs-high spots were enriched with T cells, B cells, dendritic cells (DCs), and macrophages in contrast to the TLSs-low spots (figure 1A,B). In addition, we found high expression of CD3D (T-cell marker), CD79A (B cell marker), HLA-DQA1 (DC marker), and CD68 (macrophage marker) in TLSs-high regions (online supplemental figure S1F,G).

Collectively, these results reveal that intratumoral TLSs are associated with improved prognosis and the efficacy of immunochemotherapy. Besides, immunochemotherapy could induce TLS formation and maturation. However, what are the key elements that contribute to TLS formation and maturation in the immune microenvironment?

### CXCL13<sup>+</sup> CD160<sup>+</sup> CD8<sup>+</sup> T cells and CXCL13<sup>+</sup> PDCD1<sup>+</sup> CD4<sup>+</sup> T cells were critical factors to promote TLS formation or maturation

We performed an integrative analysis of large-scale single-cell transcriptomes across six data sets using the scVI algorithm and re-clustered T cells and identified ten distinct subsets according to their differential genes (figure 1C,D). These T-cell subsets included C0-KLRC1 CD8<sup>+</sup> T subsets, C1-CCR6 CD4<sup>+</sup> T subsets, C2-GZMK CD8<sup>+</sup> T subsets, C3-FOXP3 CD4<sup>+</sup> T subsets, C4-GNLY CD8<sup>+</sup> T subsets, C5-CCR7 CD4<sup>+</sup> T subsets, C6-CXCL13 CD8<sup>+</sup> T subsets, C7-TNF CD8<sup>+</sup> T subsets, C8-CXCL13 CD4<sup>+</sup> T subsets, and C9-IL17A CD4<sup>+</sup> T subsets. Among these subsets, CD4-C8-CXCL13 and CD8-C6-CXCL13 were characterized by upregulated expression of CXCL13.

According to the literature reports, we reclassified T cells in patients with gastric cancer into naïve T cells, cytotoxic T cells, dysfunctional T cells, inhibitory T cells, proliferative T cells, effective T cells, and resident T cells based on their molecular features. CD4-C8-CXCL13 and

**Table 2** Association between TLS scores and clinicopathological features in patients with gastric cancer

Variable	Overall (%)	TLSs		$\chi^2$	P value
		Low, no. cases	High, no. cases		
	116 (100)	58	58		
Age				0.037	0.848
< 60	43 (37.1)	22	21		
≥60	73 (62.9)	36	37		
Gender				1.694	0.193
Male	61 (52.6)	31	24		
Female	55 (47.4)	27	34		
Clinical stage				4.386	0.112
II	34 (29.3)	12	22		
III	50 (43.1)	27	23		
IV	32 (27.6)	19	13		
T classification				5.224	0.073
T2	38 (32.8)	15	23		
T3	55 (47.4)	27	28		
T4	23 (19.8)	16	7		
N classification				7.172	0.067
N0	15 (12.9)	8	7		
N1	36 (31.0)	12	24		
N2	38 (32.8)	20	18		
N3	27 (23.3)	18	9		
Metastasis				1.487	0.223
No	104 (89.7)	50	54		
Yes	12 (10.3)	8	4		
Pathologic differentiation				3.117	0.211
Well differentiated	12 (10.3)	6	6		
Moderately differentiated	53 (45.7)	22	31		
Poorly differentiated	51 (44.0)	30	21		

TLSs, tertiary lymphoid structures.

CD8-C6-CXCL13 exhibited dysfunctional and inhibitory characteristics, as they expressed inhibitory signature genes (PDCD1, TIGIT, and TOX) and co-stimulatory signature genes (CD28, ICOS, and TNFRSF18) (figure 1E,F). Notably, gene expression density analysis confirmed the specific expression distribution of CD160 and ITGAE in CD8-C6-CXCL13 and the specific expression distribution of PDCD1 in CD4-C8-CXCL13 (figure 1G, online supplemental figure S2). Analysis of the bulk RNA-seq of gastric cancer tissues from the Asian Cancer Research Group (ACRG) further confirmed that CXCL13<sup>+</sup> CD160<sup>+</sup> CD8<sup>+</sup> T cells were highly correlated with TLSs (R=0.83, p<0.0001) and CXCL13<sup>+</sup> PDCD1<sup>+</sup> CD4<sup>+</sup> T cells were highly correlated with B cells (R=0.84, p<0.0001), which are crucial components of TLSs (figure 1H-J). Besides, we found that the factions of TLSs, CXCL13<sup>+</sup> CD160<sup>+</sup> CD8<sup>+</sup> T cells, and CXCL13<sup>+</sup> PDCD1<sup>+</sup> CD4<sup>+</sup> T cells were all

associated with better survival in gastric cancer through analyzing data from the ACRG database (figure 1K).

Subsequently, we performed multiplex immunofluorescence experiments and found that TLSs colocalized with CXCL13<sup>+</sup> CD160<sup>+</sup> CD8<sup>+</sup> T cells (figure 2A,B) and CXCL13<sup>+</sup> PDCD1<sup>+</sup> CD4<sup>+</sup> T cells (figure 2C,D). Additionally, the numbers of CXCL13<sup>+</sup> CD160<sup>+</sup> CD8<sup>+</sup> T cells were significantly higher in tissues with abundant TLSs (figure 2E). Furthermore, we observed a higher density of CXCL13<sup>+</sup> CD160<sup>+</sup> CD8<sup>+</sup> T cells around mature TLSs (figure 2F). Aside from that, the ratios of CXCL13<sup>+</sup> CD160<sup>+</sup> CD8<sup>+</sup> T cells to total CD160<sup>+</sup> CD8<sup>+</sup> T cells reached 70.6% around mature TLSs (figure 2G).

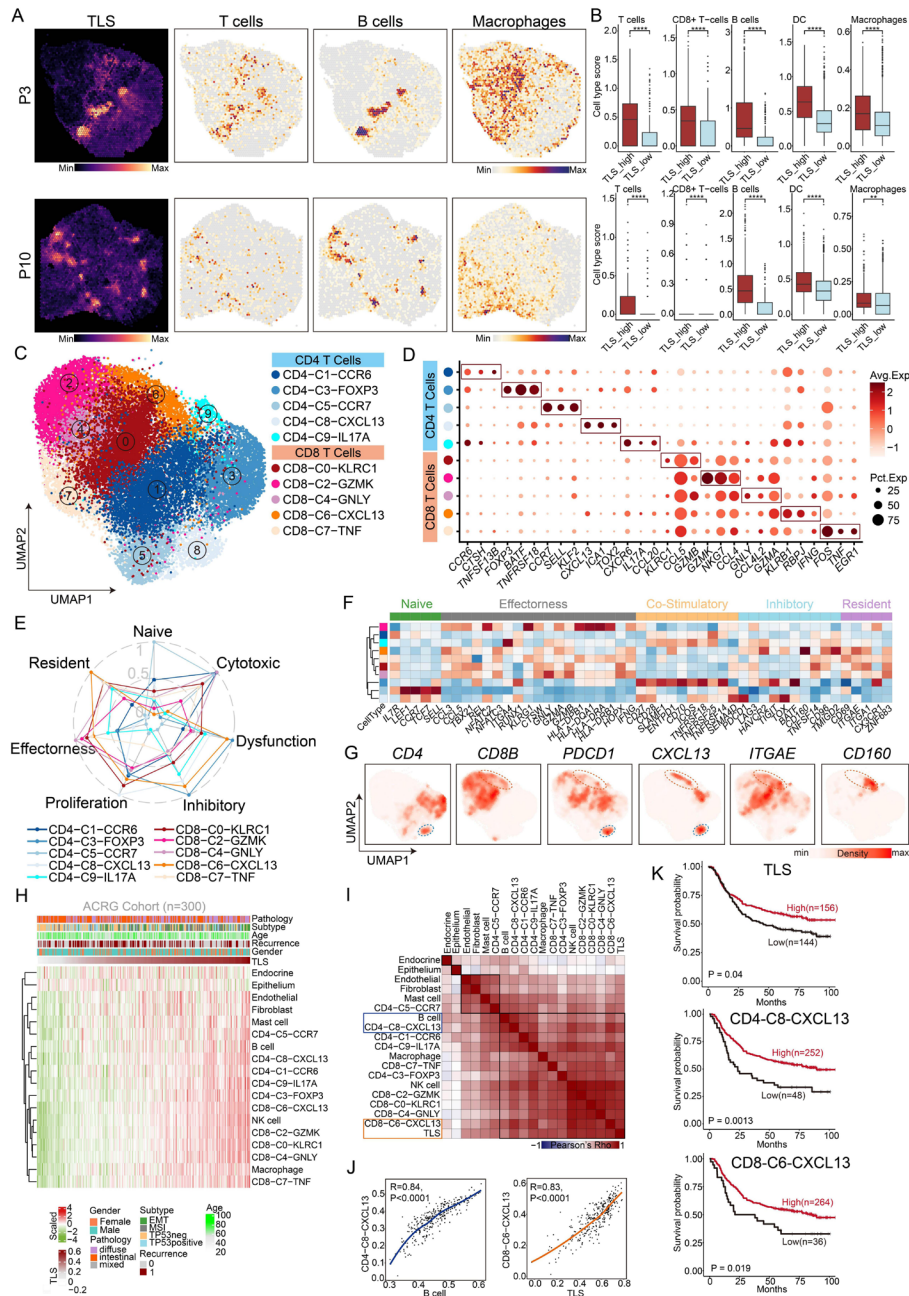


**Figure 1** Single-cell and spatial transcriptome profiling of T cells and TLSs in the tumor microenvironment of gastric cancer. (A) The spatial feature plot showing the scores of TLSs, T cells, B cells and macrophage in different patients' spatial transcriptomic data sets. P3, patient 3; P10, patient 10. (B) Comparison of the scores of different immune cells between TLS-high and TLS-low spots in different patients' spatial transcriptomic data sets. (C) UMAP plot of reclustered T cells showing 10 clusters annotated in different colors. (D) Dot plot showing the average expression levels and cell expression proportions of the differential genes in these 10 T-cell clusters. Dot size encodes the percentage of cells expressing the gene, color encodes the average per cell gene expression level. (E) CD4-C8-CXCL13 and CD8-C6-CXCL13 exhibiting dysfunctional and inhibitory characteristics. (F) The heatmap showing the characteristic gene expression in each T-cell cluster. (G) UMAP plot showing the expression of CD4, CD8B, PDCD1, CXCL13, ITGAE and CD160 in T cells. (H) The plot showing the abundance of immune cells as the score of TLSs increased using the ACRG data set. Analysis includes 300 processed samples. (I) Correlation of lineage-normalized cell-type frequencies in the ACRG cohort. (J) Scatterplot demonstrating the correlation between the CD4-C8-CXCL13 and the B cells (left panel). Scatterplot demonstrating the correlation between the CD8-C6-CXCL13 and the TLS (right panel). (K) Survival curves showing the association between factors and overall survival in patients from the ACRG cohort (log-rank test). Survival curves for TLS (upper panel), CD4-C8-CXCL13 (middle panel) and CD8-C6-CXCL13 (lower panel) and p values are shown. ACRG, Asian Cancer Research Group; TLSs, tertiary lymphoid structures; UMAP, Uniform Manifold Approximation and Projection.

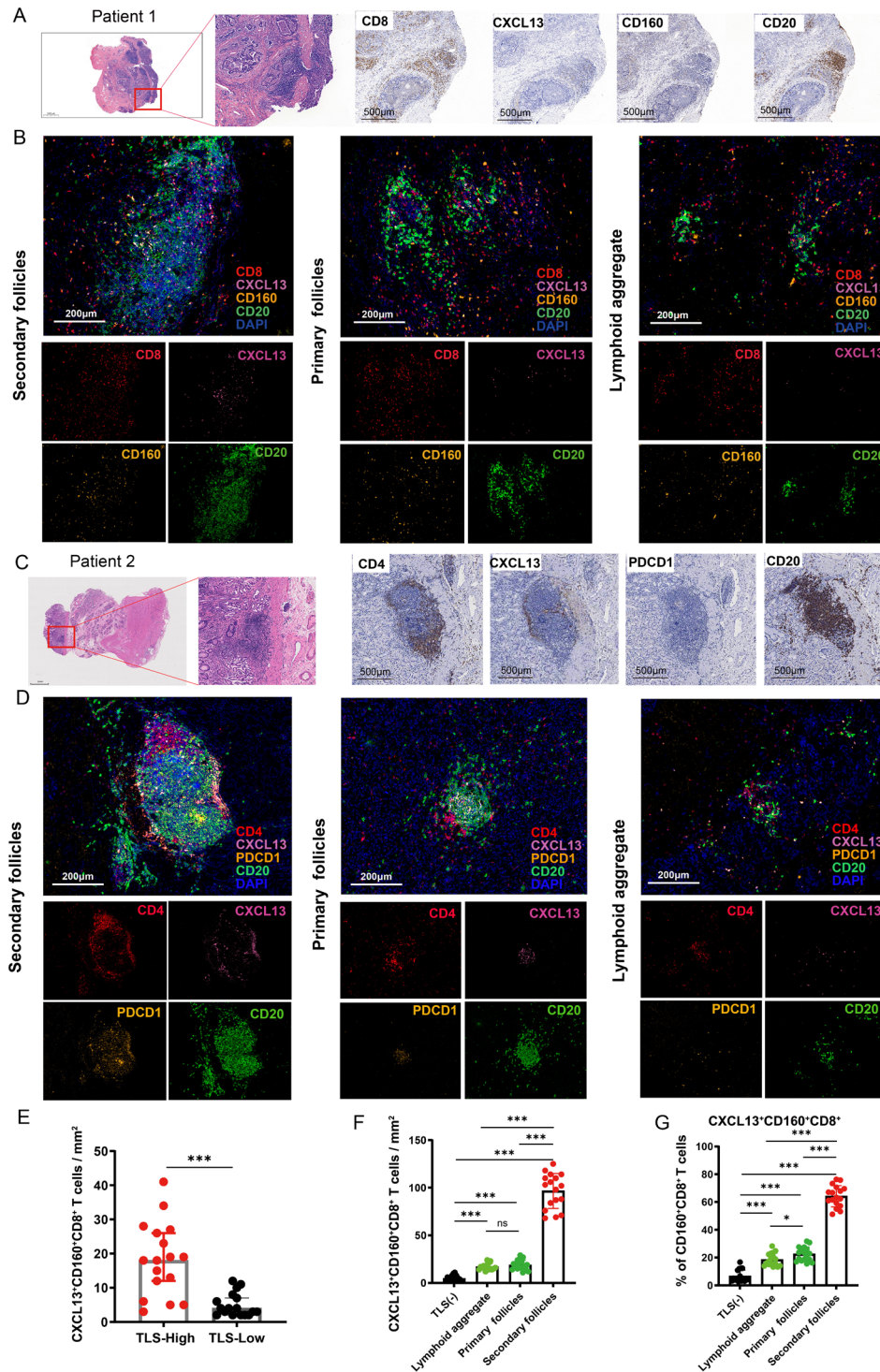


**Figure 2** CXCL13<sup>+</sup> CD160<sup>+</sup> CD8<sup>+</sup> T cells and CXCL13<sup>+</sup> PDCD1<sup>+</sup> CD4<sup>+</sup> T cell around TLSs at different stages of maturation were assessed by multiplex immunofluorescence. (A) Resected gastric tissues stained with H&E or subjected to immunohistochemistry (IHC) detection for CD8, CXCL13, CD160 and CD20. The framed areas are shown adjacently at a higher magnification. Images were captured under a light microscope. Scale bar, 500  $\mu$ m. (B) Multiplex immunofluorescence staining of human gastric cancer tissues for detection of CXCL13 (pink), CD160 (orange), CD8 (red), CD20 (green) and DAPI in gastric cancer tissues. Scale bar, 200  $\mu$ m. (C) Tumor sections stained with H&E and IHC, including CD4, CXCL13, PDCD1 and CD20. The framed areas are shown adjacently at a higher magnification. Scale bar, 500  $\mu$ m. (D) Multiplex immunofluorescence experiments were performed to detect the degree of CXCL13<sup>+</sup> PDCD1<sup>+</sup> CD4<sup>+</sup> T-cell infiltration around TLSs at different stages of maturation. Antibody panel: CXCL13 (pink), PDCD1 (orange), CD4 (red), CD20 (green). Scale bar, 200  $\mu$ m. (E) The numbers of CXCL13<sup>+</sup> CD160<sup>+</sup> CD8<sup>+</sup> T cells in patients with low (n=17) versus high (n=17) levels of TLSs were compared. (F) The density of CXCL13<sup>+</sup> CD160<sup>+</sup> CD8<sup>+</sup> T cells were higher around mature TLSs. (G) Percentage of CXCL13<sup>+</sup> CD160<sup>+</sup> CD8<sup>+</sup> T cells among CD160<sup>+</sup> CD8<sup>+</sup> T cells around TLSs at different stages of maturation. Data are presented as the mean $\pm$ SD. ns, not significant. \*p<0.05, \*\*\*p<0.001, two-tailed Student's t-test. DAPI, 4', 6-diamidino-2-phenylindole; TLSs, tertiary lymphoid structures.



### CXCL13<sup>+</sup> CD160<sup>+</sup> CD8<sup>+</sup> T cells were strongly associated with clinical response to checkpoint immunotherapy

We then analyzed transcriptome sequencing data from 45 metastatic gastric cancer tissues obtained prior to the start of PD-1 immunotherapy.<sup>11</sup> Our analysis unveiled a significant association between the extent of infiltration by CXCL13<sup>+</sup> CD160<sup>+</sup> CD8<sup>+</sup> T cells and improved immunotherapy response (figure 3A). To further explore the correlation between CXCL13<sup>+</sup> CD160<sup>+</sup> CD8<sup>+</sup> T cells and the response to immunotherapy, we performed multiplex immunofluorescence to quantify the intratumoral abundance of these cells in patients with different pathological responses. We found that responders (n=9) exhibited higher levels of CXCL13<sup>+</sup> CD160<sup>+</sup> CD8<sup>+</sup> T cells in biopsy samples obtained prior to immunotherapy compared with non-responders (n=6) (figure 3B,C,G). Therefore, the number of CXCL13<sup>+</sup> CD160<sup>+</sup> CD8<sup>+</sup> T cells may serve as an indicator of immunotherapy responsiveness. Moreover, there was a general increase in the number of intratumoral CXCL13<sup>+</sup> CD160<sup>+</sup> CD8<sup>+</sup> T cells following immunotherapy, particularly in those with a PR to therapy (figure 3D,E,G,H). However, the number of intratumoral CXCL13<sup>+</sup> CD160<sup>+</sup> CD8<sup>+</sup> T cells was decreased in patients with a CR (figure 3F, online supplemental figure S3A). This finding was consistent with the alterations observed in TLSs, suggesting a possible link to the absence of sustained antigen stimulation before detection.

Several studies have shown that CXCL13 could promote the recruitment of CXCR5<sup>+</sup> B cells into tumor site, initiating the formation or maturation of TLSs. Analysis of the bulk RNA-seq from patients with gastric cancer in The Cancer Genome Atlas revealed a strong association between CXCL13<sup>+</sup> CD160<sup>+</sup> CD8<sup>+</sup> T cells and B cells (figure 4A). Based on the integrated scRNA-seq data sets, we found CXCL13<sup>+</sup> CD160<sup>+</sup> CD8<sup>+</sup> T cells were highly correlated to B cells and might communicate with B cells through CXCL13-CXCR5 signaling (figure 4B,C). Moreover, UMAP plots showed that CXCR5 was predominantly expressed in B cells (figure 4D). Interestingly, we found that there were more CXCR5<sup>+</sup> B cells around TLSs in responders compared with non-responders after immunotherapy (figure 4E). This might be explained in part by the differential expression of CXCL13 in tissues. Additionally, we detected a higher abundance of CD38<sup>+</sup> CD138<sup>+</sup> CD27<sup>+</sup> B cells (plasma cells) in responsive tissues (figure 4F). Furthermore, our results indicated that the amounts of IgG, IgM and IgA were quite different between patients with and without responsiveness (online supplemental figure S3B). Taken together, these findings imply that CXCL13<sup>+</sup> CD160<sup>+</sup> CD8<sup>+</sup> T cells play a crucial role in influencing the formation and maturation of TLSs and are closely related to the efficacy of immunotherapy. However, what is the fine-tuning mechanism that affects CXCL13<sup>+</sup> CD160<sup>+</sup> CD8<sup>+</sup> T-cell populations?

### The activation of vitamin B<sub>6</sub> metabolic pathway could promote the expression and secretion of CXCL13 in CD160<sup>+</sup> CD8<sup>+</sup> T cells

The diverse environments encountered by T cells influence their phenotype.<sup>24</sup> CXCL13<sup>+</sup> CD160<sup>+</sup> CD8<sup>+</sup> T cells might adjust their needs to the limited tumor micro-environments. Consequently, we performed multiple metabolic feature analysis using scMetabolism, an R package for single-cell analysis. Interestingly, the results showed that vitamin B<sub>6</sub> metabolism, glutathione metabolism and oxidative phosphorylation might be crucial for CXCL13<sup>+</sup> CD160<sup>+</sup> CD8<sup>+</sup> T cells (figure 5A). PDXK, GPX4 and NDUFA4 might be putative targets, respectively (figure 5B, online supplemental figure S4A,B). We subsequently investigated the impacts of these three metabolic pathways on the immune microenvironment by ex vivo experiments using PDTFs,<sup>25</sup> which could significantly minimize immune cell loss during short-term cultures. We found that there was a significant decrease in the amount of CXCL13 released in the supernatants on the stimulation of PDXK inhibitors (ginkgotoxin) (figure 5C). Moreover, IHC results showed that high levels of PDXK expression in responsive gastric cancer tissues following immunotherapy (figure 5D). Then, the MFC murine gastric cancer cell line was used to establish subcutaneous xenograft tumor models in 615 mice. These mice were randomly assigned to four groups based on distinct treatment conditions (n=6, each group) (figure 5E). After 3 weeks, tumors were excised and measured. The results showed that the PDXK agonist (MS023) plus PD-1 inhibitors group had the smallest tumor volume and had improved survival rates, although the PDXK agonist group and the PDXK inhibitor group exhibited equivalent tumor volumes than the PBS group (figure 5F,G, online supplemental figure S4C-F). Meanwhile, the number of lymphocyte aggregates within tumors was significantly increased in PDXK agonist-treated mice (figure 5H,I).

Given that PDXK was the rate-limiting enzyme converting vitamin B<sub>6</sub> (pyridoxal) to the active form (pyridoxal phosphate), we hypothesized that vitamin B<sub>6</sub> uptake was crucial for CD160<sup>+</sup> CD8<sup>+</sup> T cells to induce CXCL13 expression and might enhance immunotherapy effects for gastric cancer. We then analyzed the cytokines and chemokines from the supernatants of PDTF cultures stimulated with vitamin B<sub>6</sub> or PD-1 inhibitors for 48 hours. We found that vitamin B<sub>6</sub>, but not PD-1 inhibitors, could significantly elevate the content of CXCL13 in the cell supernatants, as determined by ELISA (figure 6A). Through the establishment of orthotopic transplanted tumor models and MNU-induced malignant transformation models (figure 6B, online supplemental figure S4G), we observed that excessive vitamin B<sub>6</sub> supplementation augmented intratumoral CXCL13 expression and the number of TLSs (figure 6C, online supplemental figure S4H). Furthermore, vitamin B<sub>6</sub> supplementation could enhance the efficacy of PD-1 inhibitors and significantly improve survival using the tumor model of gastric orthotopic transplantation in

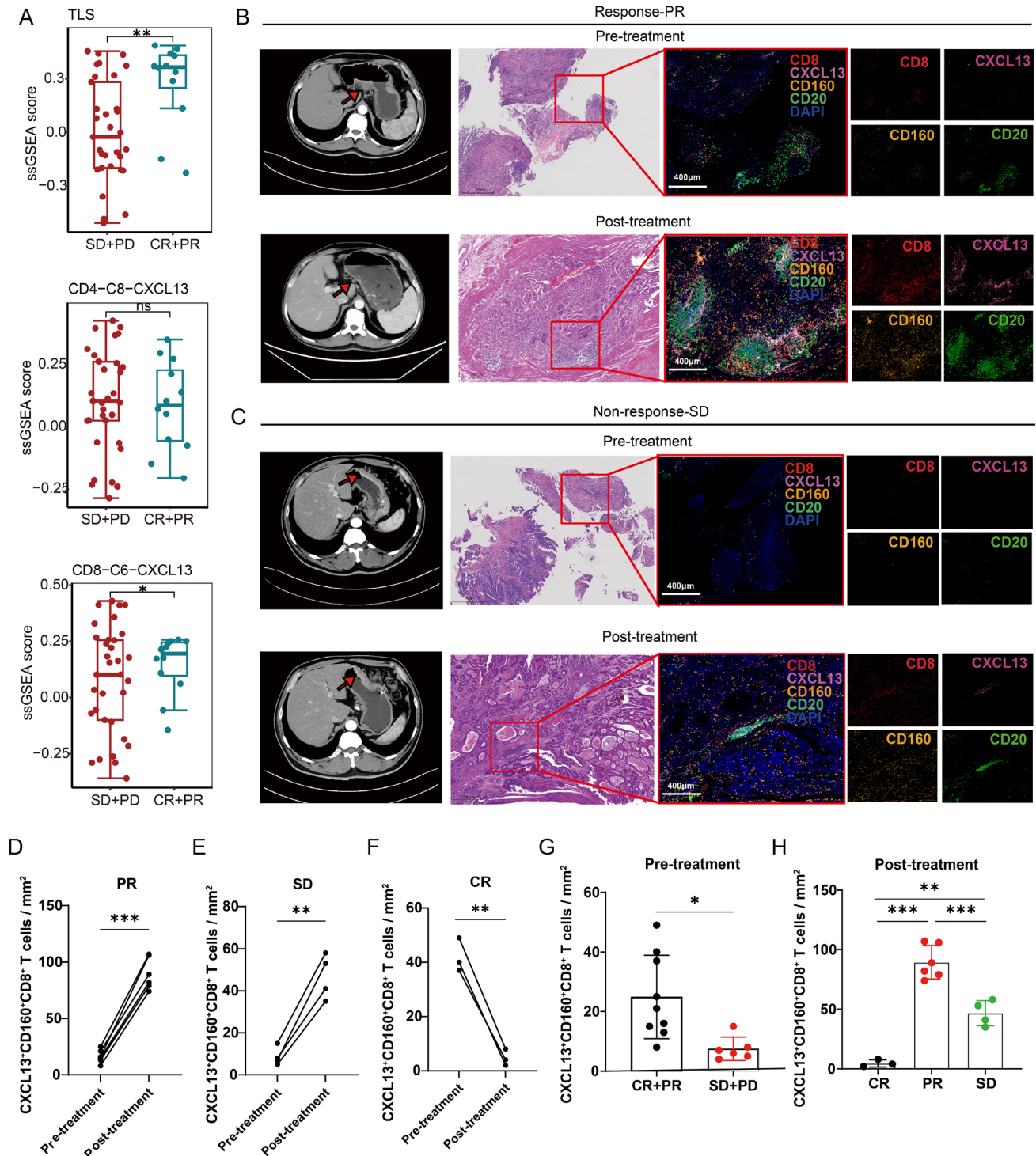


**Figure 3** CXCL13<sup>+</sup> CD160<sup>+</sup> CD8<sup>+</sup> T cells were strongly associated with clinical response to checkpoint immunotherapy. (A) Transcriptome analysis revealed that the number of TLSs and CXCL13<sup>+</sup> CD160<sup>+</sup> CD8<sup>+</sup> T cells were significantly higher in response (CR+PR) groups (n=12) compared with non-response (SD+PD) groups (n=33). (B) and (C) Enhanced CT scan of the abdomen before and after treatment with immunotherapy. The red arrows in the CT image indicate the tumor location. Multiplex immunofluorescence experiments were performed to assess the number of intratumoral CXCL13<sup>+</sup> CD160<sup>+</sup> CD8<sup>+</sup> T cells in patients with a PR or SD response. Antibody panel: CXCL13 (pink), CD160 (orange), CD8 (red), CD20 (green), scale bar, 400µm. (D–F) The Halo software was used to calculate the quantity of intratumoral CXCL13<sup>+</sup> CD160<sup>+</sup> CD8<sup>+</sup> T cells both pre-immunotherapy and post-immunotherapy across patients exhibiting varied treatment responses. (G) Comparison of the number of CXCL13<sup>+</sup> CD160<sup>+</sup> CD8<sup>+</sup> T cells between patients with CR or PR responses (n=9) and patients with SD or PD responses (n=6) prior to immunotherapy based on multiplex immunofluorescence staining. (H) Comparison of the number of infiltrating CXCL13<sup>+</sup> CD160<sup>+</sup> CD8<sup>+</sup> T cells in patients with different responses following immunotherapy. Data are presented as the mean±SD. ns, not significant. \*p<0.05, \*\*p<0.01, \*\*\*p<0.001, two-tailed Student's t-test. CR, complete response; PD, progressive disease; PR, partial response; SD, stable disease; ssGSEA, single-sample gene set enrichment analysis; TLSs, tertiary lymphoid structures.



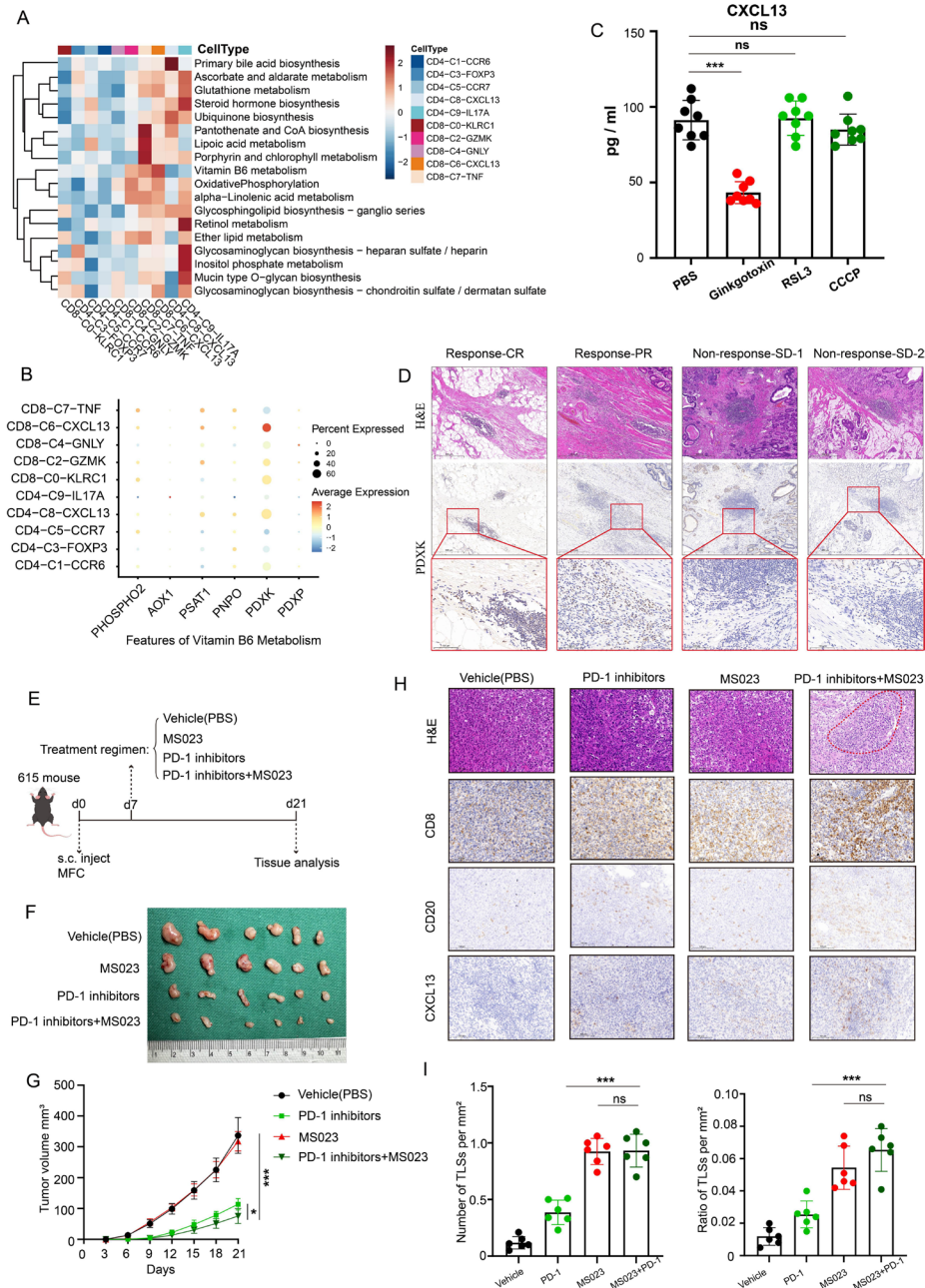


**Figure 5** Targeting PDXK could promote the formation of TLSs and enhance the efficacy of immunotherapy in gastric cancer. (A) Heatmap displaying the metabolic feature for T-cell clusters using scMetabolism package. (B) Dot plot showing the expression of the genes encoding rate-limiting enzymes of vitamin B<sub>6</sub> metabolism in different types of T cells. Dot size encodes the percentage of cells expressing the gene, color encodes the average per cell gene expression level. (C) Quantification of CXCL13 in PETFs in the presence of different enzyme inhibitors measured by ELISA. (D) Representative H&E staining and PDXK immunohistochemistry of gastric cancer tissues with different responses following immunotherapy. Scale bar, 500  $\mu$ m. (E) The schematic diagram of the animal experiments. (F–G) Images of tumors and tumor volume curves of 615 mice treated with various agents (n=6, each group). (H) Paraffin sections of mouse subcutaneous graft tumor tissue stained with H&E and IHC detection for CD8, CD20 and CXCL13. Scale bar, 100  $\mu$ m. (I) The number (left panel) and area (right panel) of TLS per tumor area were compared between groups (n=6, each group). Data are presented as the mean $\pm$ SD. ns, not significant. \* $p$ <0.05, \*\*\* $p$ <0.001, two-tailed Student's t-test. AOX1, aldehyde oxidase 1; CCCP, carbonyl cyanide m-chlorophenyl hydrazone; CR, complete response; MFC, mouse forestomach carcinoma; PBS, phosphate-buffered saline; PDXK, pyridoxal kinase; PDXP, pyridoxal phosphate; PETFs, patient-derived tumor fragments; PHOSPHO2, phosphatase orphan 2; PNPO, pyridoxamine 5'-phosphate oxidase; PR, partial response; PSAT1, phosphoserine aminotransferase 1; s.c, subcutaneous injections; SD, stable disease; TLS, tertiary lymphoid structures.

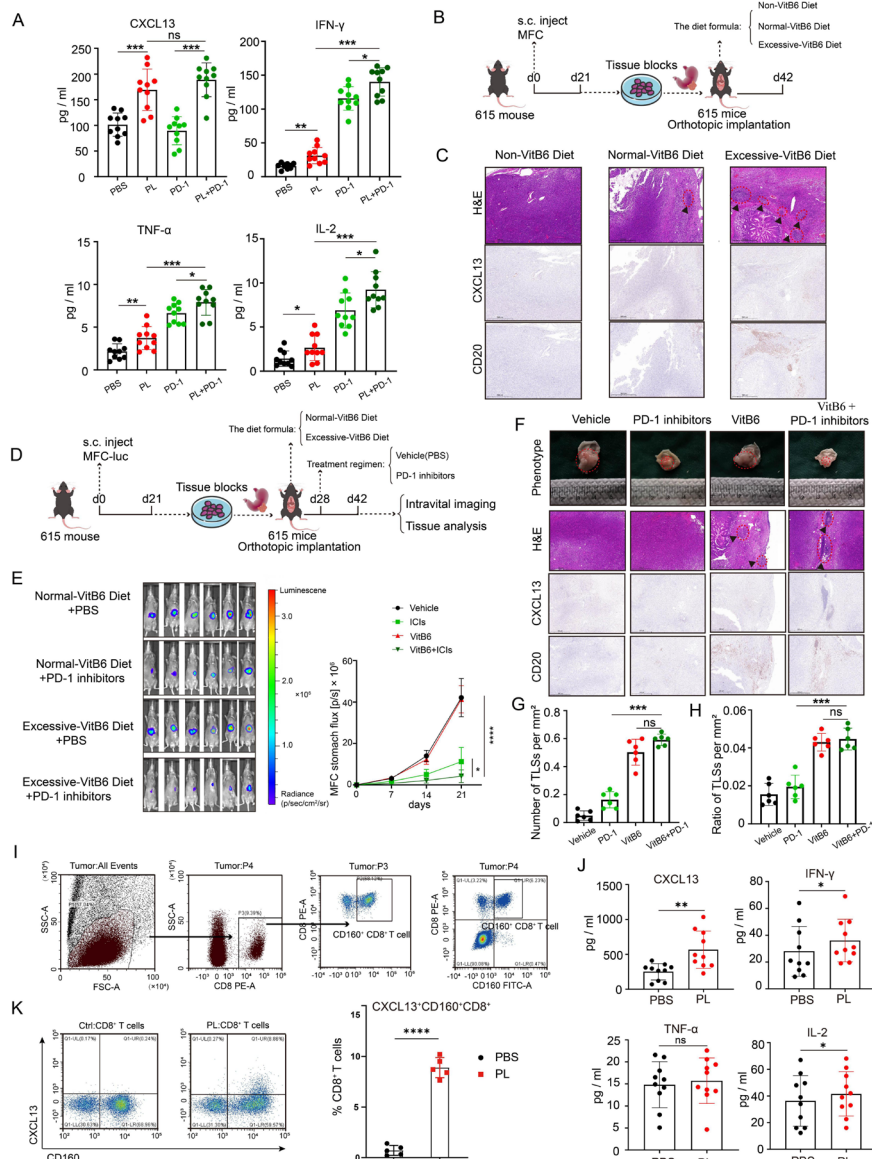


**Figure 6** Vitamin B<sub>6</sub> could promote the expression and secretion of CXCL13 in CD160<sup>+</sup> CD8<sup>+</sup> T cells. (A) Quantification of cytokine/chemokine including CXCL13, IL-2, TNF- $\alpha$  and IFN- $\gamma$ , in PDTFs in the presence of different drugs measured by ELISA. (B) The schematic diagram of orthotopic transplanted tumor model with diets containing various amounts of vitamin B<sub>6</sub> (n=6, each group). (C) Mouse orthotopic stomach xenograft tumor tissues stained with H&E and IHC detection for CD20 and CXCL13. Scale bar, 500  $\mu$ m. (D) The schematic diagram of orthotopic transplanted tumor model fed with different drugs or diets (n=6, each group). (E) The representative images of mouse bioluminescence imaging at week 3 (left panel) and the corresponding quantification analysis (right panel). (F) Representative micrographs of xenografts stained with H&E and IHC detection for CD20 and CXCL13. Scale bar, 500  $\mu$ m. (G–H) Density of TLSs (left panel) and ratio of tumor area occupied by TLSs (right panel). (I) Gating strategy for CD160<sup>+</sup> CD8<sup>+</sup> T cells. (J) Quantification of cytokine/chemokine including CXCL13, IL-2, TNF- $\alpha$  and IFN- $\gamma$ , in supernatants from CD160<sup>+</sup> CD8<sup>+</sup> T-cell cultures in the presence or absence of PL measured by ELISA. (K) Flow cytometric analysis and corresponding quantification of CXCL13<sup>+</sup> CD160<sup>+</sup> CD8<sup>+</sup> T cells with or without PL treatment. Data are presented as the mean  $\pm$  SD. ns, not significant. \*p<0.05, \*\*p<0.01, \*\*\*p<0.001, \*\*\*\*p<0.0001, two-tailed Student's t-test. ICIs, immune checkpoint inhibitors; IFN, interferon; IHC, immunohistochemistry; IL, interleukin; MFC, mouse forestomach carcinoma; PBS, phosphate-buffered saline; PL, pyridoxol; PD-1, programmed cell death protein 1; s.c, subcutaneous injections; TLS, tertiary lymphoid structures; TNF, tumor necrosis factor.

615 mice (figure 6D,E, online supplemental figure S4I). Additionally, vitamin B<sub>6</sub> plus PD-1 inhibitors could significantly lead to the activation of tumor immune microenvironment with elevated levels of lymphocyte aggregates (figure 6F–H). To investigate whether these changes were associated with CD160<sup>+</sup> CD8<sup>+</sup> T cells, we

sorted patient-derived CD160<sup>+</sup> CD8<sup>+</sup> T cells via flow cytometry and cultured them in vitro (figure 6I). Similarly, we observed a significant increase in CXCL13 release on vitamin B<sub>6</sub> stimulation, as determined by ELISA (figure 6J). In addition, flow cytometric analysis revealed an increase in the proportion of CXCL13<sup>+</sup>

CD160<sup>+</sup> CD8<sup>+</sup> T cells when the sorted CD8<sup>+</sup> T cells were stimulated with vitamin B<sub>6</sub> (figure 6K).

The results above suggest that vitamin B<sub>6</sub> metabolism plays a crucial role in promoting CXCL13 secretion in CD160<sup>+</sup> CD8<sup>+</sup> T cells. Targeting the vitamin B<sub>6</sub> metabolic pathway could be an immunomodulatory strategy for immunotherapy.

### Vitamin B<sub>6</sub> could reduce the ubiquitination modification of HIF-1 $\alpha$ by MDM2 and promote HIF-1 $\alpha$ -mediated CXCL13 transcriptional activation

We then started to explore the mechanism that vitamin B<sub>6</sub> promoted the expression and secretion of CXCL13 in CD160<sup>+</sup> CD8<sup>+</sup> T cells. We asked whether transcription factors, previously implicated in the promotion of CXCL13 expression, were induced in the presence of vitamin B<sub>6</sub>. Therefore, we treated cultured CD160<sup>+</sup> CD8<sup>+</sup> T cells with vitamin B<sub>6</sub> for 48 hours, followed by reverse transcription-PCR to assess the expression of these specific transcription factors, including SP1, HIF-1 $\alpha$ , NF $\kappa$ B and POU5F1.<sup>26</sup> The results showed that the messenger RNA level of these transcription factors had no significant alteration following vitamin B<sub>6</sub> stimulation (figure 7A, online supplemental figure S5A). Notably, only HIF-1 $\alpha$  protein levels were upregulated (figure 7B). Furthermore, we observed that the promoting effect of HIF-1 $\alpha$  on CXCL13 was attenuated by 2-MeOE2, a widely recognized HIF-1 $\alpha$  inhibitor (figure 7C). This indicated that vitamin B<sub>6</sub> might modulate CXCL13 gene expression in CD160<sup>+</sup> CD8<sup>+</sup> T cells by influencing the expression level of HIF-1 $\alpha$  protein.

Subsequently, we delved into the impact of vitamin B<sub>6</sub> on the expression of the HIF-1 $\alpha$  protein. Our findings revealed that vitamin B<sub>6</sub> still increased the half-life of HIF-1 $\alpha$  in the presence of cycloheximide, an inhibitor of de novo protein synthesis (figure 7D). Additionally, vitamin B<sub>6</sub> induced a dosage-dependent increase in HIF-1 $\alpha$  protein levels, which could be prevented by the proteasome inhibitor MG132 but not by the lysosome inhibitor NH<sub>4</sub>Cl (figure 7E,F). Aside from that, vitamin B<sub>6</sub> could reduce the ubiquitination of HIF-1 $\alpha$  (figure 7G). The results above indicated that vitamin B<sub>6</sub> could inhibit the ubiquitin-dependent proteasome degradation of HIF-1 $\alpha$ .

Literatures have reported vitamin B<sub>6</sub> could affect the ability of STUB1 and MDM2 to ubiquitinate their substrates.<sup>27 28</sup> Moreover, we found that STUB1 and MDM2 were both the possible E3 candidates that interacted with HIF-1 $\alpha$  via ubiquitin ligases/deubiquitinating enzymes-substrates interactions prediction website (<http://ubibrowser.ncpsb.org>)<sup>29</sup> (online supplemental table S2). Additionally, HIF-1 $\alpha$  interacted with both endogenous (figure 7H) and exogenous MDM2 (figure 7I), along with STUB1 (online supplemental figure S5B). Nevertheless, in HEK293T cells, vitamin B<sub>6</sub> only diminished the interaction between HIF-1 $\alpha$  and MDM2 (figure 7I, online supplemental figure S5B). Therefore, we explored whether vitamin B<sub>6</sub> influenced

HIF-1 $\alpha$  expression dependent on MDM2. We found that knockout of MDM2 led to increased HIF-1 $\alpha$  expression in HEK293T cells, and the vitamin B<sub>6</sub>-mediated increase in the HIF-1 $\alpha$  protein level was not observed (figure 7J). Furthermore, MDM2 decreased the HIF-1 $\alpha$  expression in a dose-dependent manner (figure 7K). In addition, co-transfection with MDM2 and HIF-1 $\alpha$  resulted in significant ubiquitination of HIF-1 $\alpha$  in HEK293T cells. Besides, vitamin B<sub>6</sub> decreased the level of HIF-1 $\alpha$  ubiquitination mediated by MDM2 (figure 7L). In summary, these results suggest that MDM2 interacts with HIF-1 $\alpha$  to facilitate HIF-1 $\alpha$  ubiquitination and degradation.

## DISCUSSION

There is a large population of advanced gastric cancer. These patients have poor outcomes and lack effective therapeutic options. Notably, the REGATTA (UMIN000001012) trial revealed that palliative gastrectomy plus chemotherapy did not significantly improve outcomes compared with chemotherapy alone.<sup>30</sup> This result denied the effectiveness of palliative gastrectomy as an initial therapy option for advanced gastric cancer. Recently, conversion therapy has shown significant potential value in advanced gastric cancer.<sup>8 31 32</sup> Due to continuous advancements in medical technology, PD-1 inhibitors are increasingly recognized as crucial components in conversion therapy regimens. Multiple clinical trials, such as the CheckMate-649 trial, ATTRACTION-04 trial and ORIENT-16 trial, have further confirmed the efficacy and safety of immunotherapy in unresectable stage IV gastric cancer.<sup>5-7</sup> However, there are several limitations with regarding the improvement of their effectiveness and applicability. Therefore, it is critical to develop a new approach to screen patients suitable for immunotherapy and expand indications for this regimen in clinical practice.

Our study was clinically oriented and provided a new idea for integrating clinical and basic research. In this study, we retrospectively collected medical data from fifteen patients with metastatic gastric cancer who received immunotherapy combined with chemotherapy. Additionally, we used pre-immunotherapy and post-immunotherapy tissue samples from these patients to investigate the dynamic evolution of the immune microenvironment during immunotherapy. Currently, exploring the role and function of TLSs is an emerging field of research, and TLSs are increasingly recognized as critical mediators of anti-tumor activity. However, the majority of previous studies have focused on assessing the correlations between TLSs and clinical outcomes. Despite some studies suggesting that TLSs were associated with the clinical response to immunotherapy in gastric cancer,<sup>33 34</sup> these studies have some limitations. First, although the patients with gastric cancer included in these analyzed studies received immunotherapy on tumor relapse, the tested tissue samples were all obtained from primary surgery. Second, all patients received immunotherapy as a third-line or later

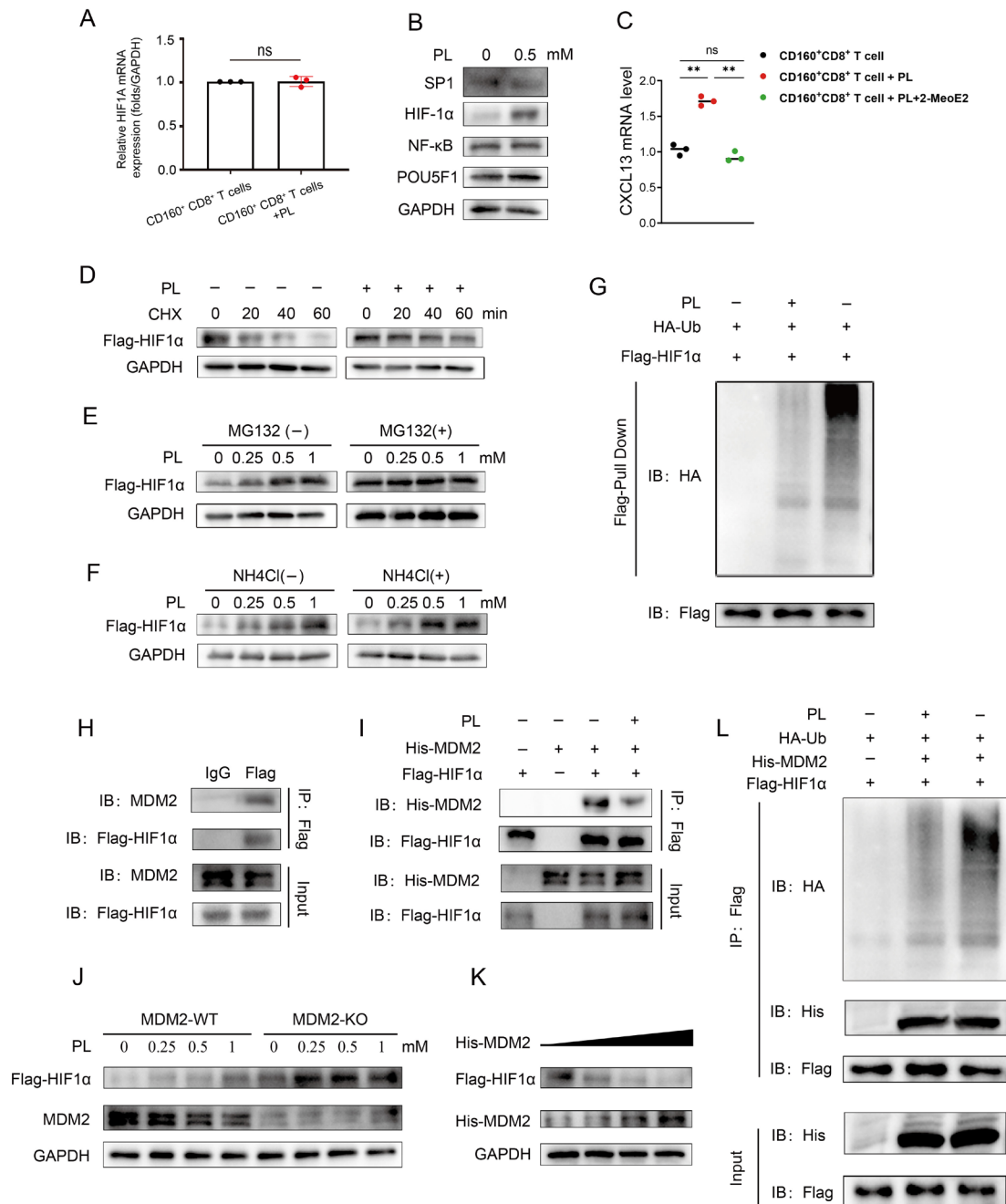


**Figure 7** Vitamin B<sub>6</sub> could reduce the ubiquitination modification of HIF-1 $\alpha$  by MDM2 and promote HIF-1 $\alpha$ -mediated CXCL13 transcriptional activation. (A) qRT-PCR analysis showing the mRNA levels of HIF-1 $\alpha$  in CD160<sup>+</sup> CD8<sup>+</sup> T cells cultured with or without PL (0.5 mM) for 48 hours. Results were normalized with GAPDH. (B) Western blot analysis showing the protein levels of SP1, HIF-1 $\alpha$ , NF- $\kappa$ B and POU5F1 in CD160<sup>+</sup> CD8<sup>+</sup> T cells cultured with or without PL (0.5 mM) for 48 hours. (C) mRNA levels of CXCL13 in CD160<sup>+</sup> CD8<sup>+</sup> T cells treated with PL (0.5 mM) alone or the combination of 2-MeoE2 (10  $\mu$ M) and PL (0.5 mM). CXCL13 mRNA was measured by qRT-PCR. Results were normalized with GAPDH. (D) HEK293T cells were cultured with or without 0.5 mM PL treatment for 48 hours and then treated with cycloheximide (20  $\mu$ g/mL) for the indicated duration. Western blot analysis of intracellular Flag-HIF-1 $\alpha$  with a Flag antibody. (E–F) HEK293T cells were treated with PL at the indicated concentrations for 48 hours and then treated with or without MG132 (10  $\mu$ M) or NH<sub>4</sub>Cl (20 mM). Western blot analysis of intracellular Flag-HIF-1 $\alpha$  with a Flag antibody. (G) Determination of the effect of PL (0.5 mM) treatment on HIF-1 $\alpha$  ubiquitination. (H–I) Co-immunoprecipitation was performed to demonstrate HIF-1 $\alpha$  interacted with endogenous and exogenous MDM2. (J) HEK293T-HIF-1 $\alpha$  or MDM2-knockout HEK293T-HIF-1 $\alpha$  cells were treated with different concentrations of PL for 48 hours. Western blot analysis of intracellular Flag-HIF-1 $\alpha$  levels. (K) HEK293T cells were transfected with Flag-HIF-1 $\alpha$  and increasing concentrations of His-MDM2. Western blot showing Flag-HIF-1 $\alpha$  and MDM2 expression. (L) HEK293T cells were transfected with the indicated plasmids for 24 hours, treated with or without 0.5 mM PL for 48 hours, and immunoprecipitated with a Flag antibody. Western blot analysis of HIF-1 $\alpha$  ubiquitination. Data are presented as the mean  $\pm$  SD. ns, not significant. \*\*p < 0.01, two-tailed Student's t-test. mRNA, messenger RNA; PL, pyridoxol; qRT-PCR, quantitative reverse transcription polymerase chain reaction; Ub, ubiquitin.

treatment. Thus, there is still insufficient robust evidence to establish the relationship between TLSs and immunotherapy responsiveness in gastric cancer. In this study, we comprehensively demonstrated that the abundance and maturation of intratumoral TLSs were associated with improved prognosis and the efficacy of immunotherapy.

Presently, there is a paucity of research concerning the mechanisms underlying TLSs. Through the analysis of single-cell data and the clinical validation, we found that CXCL13<sup>+</sup> CD160<sup>+</sup> CD8<sup>+</sup> T cells played a pivotal role in promoting the formation and maturation of TLSs. Furthermore, we discovered for the first time an association between CXCL13<sup>+</sup> CD160<sup>+</sup> CD8<sup>+</sup> T cells and the clinical response to checkpoint immunotherapy. Prior research has demonstrated that high CXCL13 expression among patients with gastric cancer correlates with improved immunotherapeutic outcomes.<sup>35</sup> It also had been reported that CD160 was crucial for the differentiation of CD8<sup>+</sup> T memory cells.<sup>36</sup> Therefore, we set out to investigate the mechanisms of CXCL13 secretion by CD160<sup>+</sup> CD8<sup>+</sup> T cells and the formation of TLSs at the levels of cells, animals and tissues. To date, such a study has not been reported.

In this study, we found for the first time that vitamin B<sub>6</sub> uptake was important for CD160<sup>+</sup> CD8<sup>+</sup> T cells to induce CXCL13 expression. A meta-analysis has indicated that high-dose vitamin B<sub>6</sub> supplementation may mitigate the risk of gastric cancer.<sup>37</sup> Additionally, multiple authoritative journals have also reported that dietary supplementation with vitamin B<sub>6</sub> can enhance immune function.<sup>38</sup> Furthermore, some studies have pointed out that vitamin B<sub>6</sub> metabolism is strongly correlated with the proliferation and functionality of CD8<sup>+</sup> effector T cells.<sup>39</sup> Nevertheless, the role of vitamin B<sub>6</sub> in tumor immunotherapy remains unexplored. Our further experiment demonstrated for the first time that vitamin B<sub>6</sub> supplementation or targeting PDXK could enhance the efficacy of PD-1 inhibitors. The findings of our studies hold significant clinical implications for immunotherapeutic applications and could provide novel ideas about TLS-inducing agents.

Of note, we found that although the number of TLSs within the tumor increased in the MS023 monotherapy group or high vitamin B<sub>6</sub> diet group (without the treatment of immunotherapy), there was no significant difference in tumor size compared with the control group *in vivo*. In fact, there are no reports in the literature indicating a definite linear relationship between TLS density and tumor size. The tumor microenvironment is composed of a variety of cells including protumorigenic immune cells, such as M2 macrophages, regulatory T cells, and myeloid-derived suppressor cells.<sup>40</sup> TLSs are also regulated by these immunosuppressive factors.<sup>41</sup> Previous research using animal models has found that tumor progression was associated with the infiltration of regulatory T cells (Tregs), rather than TLSs, and these Tregs were predominantly located in the T-cell zones of TLSs.<sup>42</sup> Therefore, the above result is reasonable. Furthermore, the survival outcomes in mice appeared to be inconsistent with

clinical statistical results. The MS023 monotherapy group and high vitamin B<sub>6</sub> diet group (without the treatment of immunotherapy) did not enhance the survival time of mice compared with the control group. We think this may be related to immunotherapy or chemotherapy because appropriate adjuvant therapy is commonly administered postoperatively in clinical practice for gastric cancer, except for early gastric cancer (T1a).<sup>43</sup>

Furthermore, for the first time, we discovered that vitamin B<sub>6</sub> could inhibit the binding of MDM2 to HIF-1 $\alpha$ , thereby decreasing the ubiquitination and degradation of HIF-1 $\alpha$  by MDM2. HIF1A is a well-known oncogene involved in the adaptive metabolic response to hypoxia, contributing to increased tumor cell growth.<sup>44</sup> However, HIF1A is equally important for the survival of immune cells in a hypoxic environment.<sup>45 46</sup> In our study, we demonstrated that HIF1A was critical for CXCL13<sup>+</sup> CD160<sup>+</sup> CD8<sup>+</sup> T cells and TLS formation.

Several limitations exist in this study. First, this study was retrospective and conducted at a single center, and the number of sample cases was too small to construct a predictive model. Second, the exact mechanism of the direct interaction between vitamin B<sub>6</sub> and MDM2 remains to be investigated. Third, although bioinformatic analysis supported a strong link between CXCL13<sup>+</sup> CD160<sup>+</sup> CD8<sup>+</sup> T cells and CXCR5<sup>+</sup> cells through CXCL13-CXCR5 signaling pathway, further studies are needed to demonstrate whether CXCL13 derived from CD160<sup>+</sup> CD8<sup>+</sup> T cells exerts a chemotactic effect on CXCR5<sup>+</sup> B cells *in vitro* and *in vivo*. There was evidence of the critical role of CXCL13-CXCR5 signaling axis in regulating B-cell activation.<sup>47</sup> Nonetheless, further investigation is required to determine the influence of CXCL13<sup>+</sup> CD160<sup>+</sup> CD8<sup>+</sup> T cells on B-cell differentiation and function.

In summary, our study was the first to propose that the number and maturity of TLSs, along with the extent of CXCL13<sup>+</sup> CD160<sup>+</sup> CD8<sup>+</sup> T cell infiltration, could serve as biomarkers for immunotherapy in gastric cancer. We also identified that vitamin B<sub>6</sub> supplementation could substantially enhance the efficacies of cancer immunotherapies. Moreover, we demonstrated vitamin B<sub>6</sub> could promote the secretion of CXCL13 by CD160<sup>+</sup> CD8<sup>+</sup> T cells by reducing the degradation of HIF-1 $\alpha$ , thereby promoting the formation of TLSs (online supplemental figure S6). Our study was expected to refine the theory of immunotherapy and shed important new light on the clinical application of a more effective immunotherapy for advanced gastric cancer.

**Acknowledgements** Our special acknowledgments to Xuehui Long for experimental guidance.

**Contributors** LY and JW performed the study concept and design. JW and YLiang drafted and revised the initial manuscript. JW performed most of the animal-based experiments. YLiang analyzed spatial transcriptomics data and integrated single-cell data. JX and AX assisted with the experiments. All authors participated in gathering and analyzing the data. LY takes responsibility for these results. Guarantor: LY.

**Funding** This study was supported by the Jiangsu Province Capability Improvement Project through Science, Technology, and Education (Jiangsu



Provincial Medical Key Discipline, ZDXK202222) and the National Natural Science Foundation of China (Grant No. 81874219).

**Competing interests** None declared.

**Patient consent for publication** Not applicable.

**Ethics approval** Human gastric cancer were collected with permission from the Ethics Committee of the First Affiliated Hospital of Nanjing Medical University (no.2022-SR-597). Participants gave informed consent to participate in the study before taking part.

**Provenance and peer review** Not commissioned; externally peer reviewed.

**Data availability statement** Data are available upon reasonable request.

**Supplemental material** This content has been supplied by the author(s). It has not been vetted by BMJ Publishing Group Limited (BMJ) and may not have been peer-reviewed. Any opinions or recommendations discussed are solely those of the author(s) and are not endorsed by BMJ. BMJ disclaims all liability and responsibility arising from any reliance placed on the content. Where the content includes any translated material, BMJ does not warrant the accuracy and reliability of the translations (including but not limited to local regulations, clinical guidelines, terminology, drug names and drug dosages), and is not responsible for any error and/or omissions arising from translation and adaptation or otherwise.

**Open access** This is an open access article distributed in accordance with the Creative Commons Attribution Non Commercial (CC BY-NC 4.0) license, which permits others to distribute, remix, adapt, build upon this work non-commercially, and license their derivative works on different terms, provided the original work is properly cited, appropriate credit is given, any changes made indicated, and the use is non-commercial. See <http://creativecommons.org/licenses/by-nc/4.0/>.

#### ORCID iDs

Yuan Liang <http://orcid.org/0009-0000-5758-4906>

Li Yang <http://orcid.org/0000-0001-5456-1944>

#### REFERENCES

- Sung H, Ferlay J, Siegel RL, *et al*. Global Cancer Statistics 2020: GLOBOCAN Estimates of Incidence and Mortality Worldwide for 36 Cancers in 185 Countries. *CA Cancer J Clin* 2021;71:209–49.
- Alsina M, Arrazubi V, Diez M, *et al*. Current developments in gastric cancer: from molecular profiling to treatment strategy. *Nat Rev Gastroenterol Hepatol* 2023;20:155–70.
- Xu R, Arkenau T, Bang Y, *et al*. P-26 RATIONALE 305: Tislelizumab plus chemotherapy versus placebo plus chemotherapy as first-line therapy in patients with gastric or gastroesophageal junction adenocarcinoma. *Ann Oncol* 2020;31:S97–8.
- Rha SY, Oh D-Y, Yañez P, *et al*. Pembrolizumab plus chemotherapy versus placebo plus chemotherapy for HER2-negative advanced gastric cancer (KEYNOTE-859): a multicentre, randomised, double-blind, phase 3 trial. *Lancet Oncol* 2023;24:1181–95.
- Kang Y-K, Chen L-T, Ryu M-H, *et al*. Nivolumab plus chemotherapy versus placebo plus chemotherapy in patients with HER2-negative, untreated, unresectable advanced or recurrent gastric or gastro-oesophageal junction cancer (ATTRACTION-4): a randomised, multicentre, double-blind, placebo-controlled, phase 3 trial. *Lancet Oncol* 2022;23:234–47.
- Janjigian YY, Shitara K, Moehler M, *et al*. First-line nivolumab plus chemotherapy versus chemotherapy alone for advanced gastric, gastro-oesophageal junction, and oesophageal adenocarcinoma (CheckMate 649): a randomised, open-label, phase 3 trial. *Lancet* 2021;398:27–40.
- Xu J, Jiang H, Pan Y, *et al*. Sintilimab Plus Chemotherapy for Unresectable Gastric or Gastroesophageal Junction Cancer: The ORIENT-16 Randomized Clinical Trial. *JAMA* 2023;330:2064–74.
- Liang H, Yan X, Li Z, *et al*. Clinical outcomes of conversion surgery following immune checkpoint inhibitors and chemotherapy in stage IV gastric cancer. *Int J Surg* 2023;109:4162–72.
- Yoshida K, Yasufuku I, Terashima M, *et al*. International Retrospective Cohort Study of Conversion Therapy for Stage IV Gastric Cancer 1 (CONVO-GC-1). *Ann Gastroenterol Surg* 2022;6:227–40.
- Li Y-J, Liu X-Z, Yao Y-F, *et al*. Efficacy and safety of preoperative immunotherapy in patients with mismatch repair-deficient or microsatellite instability-high gastrointestinal malignancies. *World J Gastrointest Surg* 2023;15:222–33.
- Kim ST, Cristescu R, Bass AJ, *et al*. Comprehensive molecular characterization of clinical responses to PD-1 inhibition in metastatic gastric cancer. *Nat Med* 2018;24:1449–58.
- Wu H, Estrella V, Beatty M, *et al*. T-cells produce acidic niches in lymph nodes to suppress their own effector functions. *Nat Commun* 2020;11:4113.
- Li Z, Jiang Y, Li B, *et al*. Development and Validation of a Machine Learning Model for Detection and Classification of Tertiary Lymphoid Structures in Gastrointestinal Cancers. *JAMA Netw Open* 2023;6:e2252553.
- Kemi N, Ylitalo O, Väyrynen JP, *et al*. Tertiary lymphoid structures and gastric cancer prognosis. *APMIS* 2023;131:19–25.
- Cabrita R, Lauss M, Sanna A, *et al*. Tertiary lymphoid structures improve immunotherapy and survival in melanoma. *Nature New Biol* 2020;577:561–5.
- Helmink BA, Reddy SM, Gao J, *et al*. B cells and tertiary lymphoid structures promote immunotherapy response. *Nature New Biol* 2020;577:549–55.
- Gavriatou N, Fortis E, Spathis A, *et al*. B-cell infiltration is associated with survival outcomes following programmed cell death protein 1 inhibition in head and neck squamous cell carcinoma. *Ann Oncol* 2024;35:340–50.
- Petitprez F, de Reyniès A, Keung EZ, *et al*. B cells are associated with survival and immunotherapy response in sarcoma. *Nature New Biol* 2020;577:556–60.
- Schumacher TN, Thommen DS. Tertiary lymphoid structures in cancer. *Science* 2022;375:eabf9419.
- Chen J, Liu K, Luo Y, *et al*. Single-Cell Profiling of Tumor Immune Microenvironment Reveals Immune Irresponsiveness in Gastric Signet-Ring Cell Carcinoma. *Gastroenterology* 2023;165:88–103.
- Kinker GS, Vitiello GAF, Diniz AB, *et al*. Mature tertiary lymphoid structures are key niches of tumour-specific immune responses in pancreatic ductal adenocarcinomas. *Gut* 2023;72:1927–41.
- Ukita M, Hamanishi J, Yoshitomi H, *et al*. CXCL13-producing CD4+ T cells accumulate in the early phase of tertiary lymphoid structures in ovarian cancer. *JCI Insight* 2022;7:e157215.
- Wu R, Guo W, Qiu X, *et al*. Comprehensive analysis of spatial architecture in primary liver cancer. *Sci Adv* 2021;7:eabg3750.
- Wilfahrt D, Delgoffe GM. Metabolic waypoints during T cell differentiation. *Nat Immunol* 2024;25:206–17.
- Voabil P, de Buijn M, Roelofsen LM, *et al*. An ex vivo tumor fragment platform to dissect response to PD-1 blockade in cancer. *Nat Med* 2021;27:1250–61.
- Zhou L, Kong G, Palmisano I, *et al*. Reversible CD8 T cell-neuron cross-talk causes aging-dependent neuronal regenerative decline. *Science* 2022;376:eabd5926.
- Zhu S, Zhong S, Cheng K, *et al*. Vitamin B6 regulates IL-33 homeostasis to alleviate type 2 inflammation. *Cell Mol Immunol* 2023;20:794–807.
- Yuan J, Li J, Shang M, *et al*. Identification of vitamin B6 as a PD-L1 suppressor and an adjuvant for cancer immunotherapy. *Biochem Biophys Res Commun* 2021;561:187–94.
- Wang X, Li Y, He M, *et al*. UbiBrowser 2.0: a comprehensive resource for proteome-wide known and predicted ubiquitin ligase/deubiquitinase-substrate interactions in eukaryotic species. *Nucleic Acids Res* 2022;50:D719–28.
- Fujitani K, Yang H-K, Mizusawa J, *et al*. Gastrectomy plus chemotherapy versus chemotherapy alone for advanced gastric cancer with a single non-curable factor (REGATTA): a phase 3, randomised controlled trial. *Lancet Oncol* 2016;17:309–18.
- Hu C, Terashima M, Cheng X. Conversion therapy for stage IV gastric cancer. *Sci Bull (Beijing)* 2023;68:653–6.
- Solaini L, Ministrini S, Bencivenga M, *et al*. Conversion gastrectomy for stage IV unresectable gastric cancer: a GIRCG retrospective cohort study. *Gastric Cancer* 2019;22:1285–93.
- Jiang Q, Tian C, Wu H, *et al*. Tertiary lymphoid structure patterns predicted anti-PD1 therapeutic responses in gastric cancer. *Chin J Cancer Res* 2022;34:365–82.
- Mori T, Tanaka H, Deguchi S, *et al*. Clinical efficacy of nivolumab is associated with tertiary lymphoid structures in surgically resected primary tumors of recurrent gastric cancer. *PLoS ONE* 2022;17:e0262455.
- Yang M, Lu J, Zhang G, *et al*. CXCL13 shapes immunoreactive tumor microenvironment and enhances the efficacy of PD-1 checkpoint blockade in high-grade serous ovarian cancer. *J Immunother Cancer* 2021;9:e001136.
- Zhang L, Zhang A, Zhu X, *et al*. CD160 Signaling Is Essential for CD8+ T Cell Memory Formation via Upregulation of 4-1BB. *J Immunol* 2023;211:1367–75.
- Mocellin S, Briarava M, Pilati P. Vitamin B6 and Cancer Risk: A Field Synopsis and Meta-Analysis. *J Natl Cancer Inst* 2017;109:1–9.
- He C, Wang D, Shukla SK, *et al*. Data from Vitamin B6 Competition in the Tumor Microenvironment Hampers Antitumor Functions of NK Cells. *Cancer Discov* 2023.



- 39 Bargiela D, Cunha PP, Veliça P, *et al.* Vitamin B6 Metabolism Determines T Cell Anti-Tumor Responses. *Front Immunol* 2022;13:837669.
- 40 de Visser KE, Joyce JA. The evolving tumor microenvironment: From cancer initiation to metastatic outgrowth. *Cancer Cell* 2023;41:374–403.
- 41 Sautès-Fridman C, Fridman WH. TLS in Tumors: What Lies Within. *Trends Immunol* 2016;37:1–2.
- 42 Joshi NS, Akama-Garren EH, Lu Y, *et al.* Regulatory T Cells in Tumor-Associated Tertiary Lymphoid Structures Suppress Anti-tumor T Cell Responses. *Immunity* 2015;43:579–90.
- 43 Wang F-H, Zhang X-T, Tang L, *et al.* The Chinese Society of Clinical Oncology (CSCO): Clinical guidelines for the diagnosis and treatment of gastric cancer, 2023. *Cancer Commun (Lond)* 2024;44:127–72.
- 44 Semenza GL. Targeting HIF-1 for cancer therapy. *Nat Rev Cancer* 2003;3:721–32.
- 45 Palazon A, Tyrakis PA, Macias D, *et al.* An HIF-1 $\alpha$ /VEGF-A Axis in Cytotoxic T Cells Regulates Tumor Progression. *Cancer Cell* 2017;32:669–83.
- 46 Roy S, Rizvi ZA, Clarke AJ, *et al.* EGFR-HIF1 $\alpha$  signaling positively regulates the differentiation of IL-9 producing T helper cells. *Nat Commun* 2021;12:3182.
- 47 Sáez de Guinoa J, Barrio L, Mellado M, *et al.* CXCL13/CXCR5 signaling enhances BCR-triggered B-cell activation by shaping cell dynamics. *Blood* 2011;118:1560–9.